Korean J. of Chem. Eng., **7**(1) (1990) *22-30*

LIQUID-LIQUID MIXING FOR THE BREAKUP OF ACCELERATING DROPS

Ji-Won YANG and Hyun-Soo YANG*

Department of Chemical Engineering, Korea Institute of Technology
*Department of Chemical Engineering, Chungnam National University
(Received 22 February 1989 • accepted 18 September 1989)

Abstract—Studies have been made on the fragmentation of liquid metal drops falling through a water-glycerine mixture containing small amounts of nitrogen bubbles owing to the passage of a strong shock wave. The apparent drop volume increased with time, but neither stripping of small droplets nor misty wake formation was observed in the high-speed photographs. The drop flattened initially into a spherical cap which increased in radius, but remained smooth, within the time period of interest. Hence the Taylor instability is not the principal fragmentation mechanism at these Weber numbers (5-644). Entrainment of liquid into the drop was the cause of breakup, and was postulated to be due to turbulent mixing resulting from vorticity generation near the plane of separation. A hydrodynamic fragmentation model was developed which predicts the rate of drop volume increase reasonably well. The breakup time constant was presented, and drop trajectory can also be predicted from the model.

INTRODUCTION

Among safety issues for nuclear reactors, a main concern is an understanding of the consequences of a hypothetical core disruptive accident, which may lead to fuel melting and subsequent thermal interaction of hot molten fuel with coolant. The destructive shock wave forces resulting from the explosive energy release may be responsible for the ruptures of fuel channels that led to the destruction of the core of Chernobyl Unit 4 and the direct release of radioactivity to the atmosphere. The following four-stage processes have been generally believed to be a coherent feature of the fuel-coolant interactions [1]: 1) Coarse premixing of fuel and coolant without rapid heat transfer, which requires stable film boiling, when the two liquids come into contact; 2) Triggering event that consists of vapor film collapse in some small region due to arrival of an external pressure shock or cooling of the hot liquid; 3) Escalation of the fuel-coolant interaction by a cyclic mixing process, in which fragmentation and energy transfer occur simultaneously; 4) Propagation of a fully-developed detonation wave through the coarse fuel-coolant mixture.

At present, the details of each stage, especially in regard to fragmentation and mixing of fuel and coolant, are being disputed. Among various fragmentation mechanisms proposed, two broad categories can be classified: the spontaneous nucleation theory [2] and the thermal detonation model [3]. The former theory has been the basis of the boiling fragmentation mechanism, while the latter model has been the ground of the purely hydrodynamic fragmentation mechanism. The spontaneous nucleation theory states that the contact interface temperature must exceed the spontaneous nucleation temperature for violent interactions to occur. The thermal detonation model treats the shock as a plane, steady one-dimensional wave proceeding through initially coarsely-mixed fuel and coolant. Since vapor explosions are supposed to be prevented by pressure suppression in the Light Water Reactor and by low contact interface temperature in the Liquid Metal Fast Breeder Reactor according to the nucleation concept, the thermal detonation theory is postulated to explain the phenomena at supercritical pressures without considering vapor bubble nucleation. Extensive works on the thermal interaction can be found in literatures. In the following a brief review is given on the hydrodynamic fragmentation studies.

Defining the dimensionless breakup time by

$$T_b = \left(\frac{t_b u_r}{d_o}\right) \cdot \varepsilon^{1/2} \tag{1}$$

where u_r is the relative velocity, d_o is the initial drop diameter, and ε is the density ratio of the continuous phase (gas) to the dispersed phase (liquid), Ranger and

Nicholls [4] found that $T_b = 5$. The breakup time definition was based on the time required to produce only a trace of mist. Harper et al. [5] computed the windward surface Talor instability of an accelerating drop. The critical Bond number $Bo = \rho_f a r_o^2/\sigma$, below which the drop vibrated without breakup, was found to be 11. For $Bo > O(10^5)$, the surface wave growth rate was dominated by acceleration, and the unstable Taylor wave pierced the drop before it had sufficient time to distort. Simpkins and Bales [6] examinec water drop breakup with helium and hydrogen gas shocks of Mach numbers of 2-9 and Weber numbers of about 6×10^3-1.1×10^6. The onset of Taylor instability was correlated by

$$T_b = 11 Bo^{-1/4} \quad (2)$$

which represented the lower bound of the breakup time, and was consistent with the observations of Reinecke and Waldman [7].

Patel and Theofanous [8] investigated the hydrodynamic fragmentation of acetylene tetrabromide, mercury and gallium drops in a vertical shock tube capable of operation up to 60 MPa. The breakup times obtained were shorter than those observed in gas-liquid systems (especially for initially disturbed drops). The proportionality constant between $Bo^{-1/4}$ and the dimensionless breakup time, T_b, was found to be between one and four, corresponding to the initiation of breakup and substantial fragmentation, respectively. Baines and Buttery [9] observed the breakup of a mercury drop in a closed vessel full of water which was impulsively raised to a high velocity. The range of Weber numbers studied was from 100 to 2000 for mercury drops of about 5 mm in diameter. The dimensionless breakup time was found to be $T_b = 3$ to 5 for that range. Both boundary layer stripping and surface wave instabilities were observed. Taylor instabilities at the front surface of the drop were reported to be operative only for Weber numbers around 2000. The fragmentation of gallium drops in water at We = 30-3520 was investigated by Kim et al. [10] by an exploding wire technique. The shear flow of the water was seen to be the cause of the stripping of fragments in the form of a closed thin gallium skin or shreds of skins. The dimensionless fragmentation time based on complete breakup was found to be between 3.5 and 6.6.

In the present study, the fragmentation of liquid drops behind a pressure shock wave in two-phase environment is investigated. The effects of void fraction change in two phase mixture are also studied. A qualitative description of the drop fragmentation is provided and discussed based on the high-speed photographs taken at rates up to 7,000 frames per second. The time constant for drop breakup, critical Weber number, and size of fragments are presented. A hydrodynamic fragmentation model based on the entrainment concept is developed and compared with experimental results. For measurement of fragment size, a highly nonisothermal column was prepared, in which the temperature of the lower column was below the phase transition temperature of Wood's metal. The fragment size distribution was shown and compared with other experimental data obtained in gas-liquid systems.

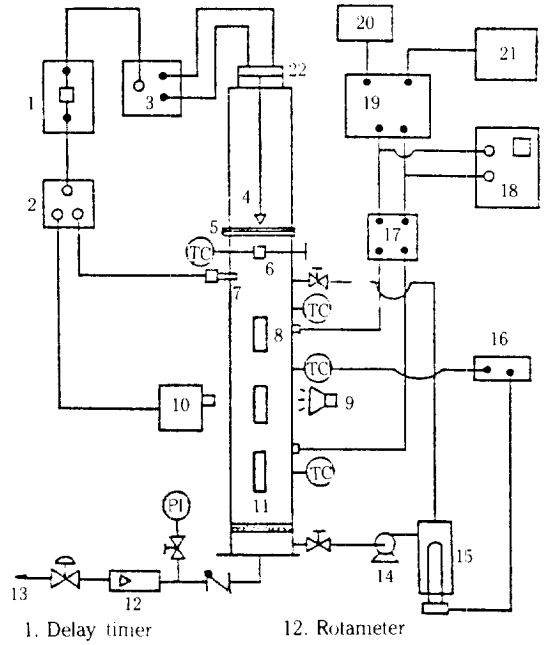

1. Delay timer
2. Event synchronizer
3. Solenoid control
4. Plunger
5. Diaphragm
6. Injector
7. Photo detector
8. Pressure transducer
9. Projection lamp
10. High speed camera
11. Gas sparger
12. Rotameter
13. Argon supply
14. Pump
15. Imersion heater
16. Temperature controller
17. Amplifier
18. Oscilloscope
19. Micro-computer
20. CRT
21. Printer
22. Linear solenoid

Fig. 1. Schematic diagram of experimental setup.

EXPERIMENTAL

Fig. 1 shows the schematic diagram of the experimental setup in Wood's metal experiments. The shock tube is capable of operation at driver pressures up to 3 MPa. Runs with mercury did not utilize the coolant heating system. The aqueous glycerol solution of

known concentration was prepared and introduced into the test section to a predetermined level. A 1 Kilowatt immersion heater located in the circulation loop was turned on. Coolant was allowed to circulate through the column by turning on the pump and the temperature controller was set at 75°C. Meanwhile, the 16 mm high-speed camera was properly placed, focused, and a roll of 100-ft film was threaded. Pressure transducer amplifiers and the microcomputer were turned on and a diskette with a proper data sampling program was inserted into disk drive. While checking the coolant temperature, the drop injector heater was turned on.

Depending upon the shock pressure desired for each experiment, proper diaphragm materials (a piece of aluminum or double layers of Mylar film) were inserted between the driver and driven section. The window in the injector port was opened and a piece of solid metal was loaded into the crucible and allowed to melt. The argon gas valve was opened to obtain the desired void fraction in the column.

The test section was isolated by closing all the valves except a normally open solenoid valve. The delay time (450 ms or 800 ms) was set on a precision timer. The trigger system was armed and the 50 volt power supply to the solenoid was turned on, thereby allowing voltage across the capacitor in the timer circuit to rise. The driver section was pressurized by supplying high pressure nitrogen from a commercial nitrogen cylinder. The molten metal temperature was measured by dipping the miniature thermocouple tip inside the crucible.

The light was turned on and the cup was tilted to allow the molten metal drop to fall. Upon detecting the passage of a drop, the photodetector would send a signal simultaneously to start the camera and to close the solenoid valve. After the specific delay time set in the timer, all the energy stored in the capacitor would discharge through the linear solenoid, thereby rupturing the diaphragm and generating a shock wave. Synchronization of events was achieved by proper delay time setting through trial and error. The film was retrieved and saved for future developing. Shock pressure histories stored in the computer were saved in a diskette as a permanent file. For the collection of the fragments it was necessary to let the particles settle down before the coolant was gently drained. The drained liquid was filtered in order to collect the smaller particles suspended in the liquid. The bulk of fragmented mass was sieved with six different sized screen meshes ranging from 1.679 mm to 0.074 mm.

Table 1. Initial experimental conditions

Run No	Initial Driver Pressure(Psig)	Shock Pressure ratio	Void fraction(%)	Drop Diameters***
* W112	200	9.65	4.17	1.4-3.3
W107	160	8.12	5.58	1.2-1.4
W303	300	19.82	4.63	4.5-5.6
W324	195	10.15	5.73	3.3
W312	195	11.17	5.78	2.5
W317	204	13.21	1.79	2.8
W154	190	10.15	3.82	3.3
W002	150	8.12	3.41	1.5-2.7
W143	120	6.09	3.09	2.8
**M167	215	9.65	0.75	2.0-3.5
M162	140	7.61	1.71	2.9
M163	140	6.09	1.29	1.2-1.4
M165	120	4.56	1.51	2.7
M159	100	3.54	2.20	1.0
M171	200	9.65	0.6	1.3-2.0
M174	200	11.68	1.2	3.3
M177	275	15.24	1.08	2.8

*: W denotes Wood's metal experiment
**: M denotes mercury experiment
***: in millimeters

RESULTS AND DISCUSSION

The initial experimental conditions are listed in Table 1. The shock pressure ratio varied from 3.54 to 19.8, the range of void fraction was from 0.6 to 5.78% and the drop diameters were between 1.0 mm and 5.6 mm. Figure 2 shows a sample shock pressure history

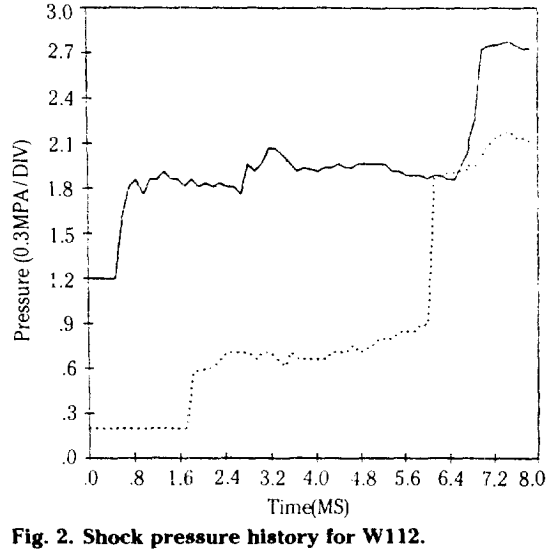

Fig. 2. Shock pressure history for W112.

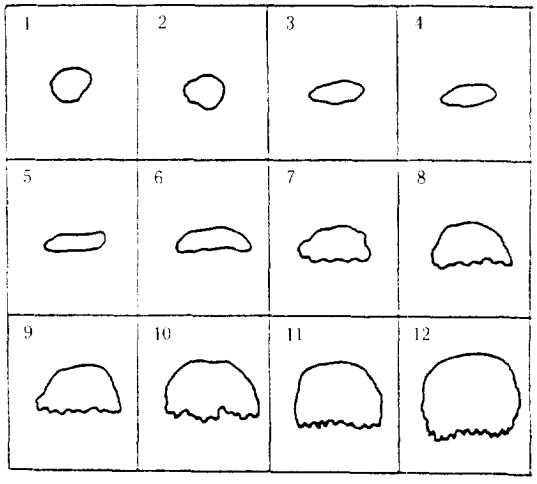

Fig. 3. Wood's metal drop responses.

Table 2. Experimental results

Drop No	d_o(mm)	C_D	E_{cf}	We	a(m/s^2)	T_b	λ_{cut}(mm)
W112-A	1.54	0.62	0.044	65	1553	2.23	1.05
W112-B	2.05	0.80	0.067	83	1467	1.4	1.08
W112-C	4.17	0.79	0.042	78	1246	2.0	1.18
W112-D	3.65	3.55	0.045	132	1147	1.12	1.23
W107-A	1.63	0.56	0.076	77	2010	0.64	0.93
W107-B	1.38	0.63	0.091	65	2218	0.69	0.88
W303-A	5.45	0.31	0.049	573	1314	1.09	1.15
W303-B	6.51	0.94	0.079	644	1365	0.75	1.12
W324-A	3.96	0.41	0.13	283	1057	0.45	1.28
W167-A	2.63	3.46	0.17	11	436	0.61	1.65
W167-B	4.02	6.80	0.23	15	530	0.37	1.50
W162-A	2.89	2.70	0.17	26	549	0.42	1.47
W163-A	1.59	2.09	0.064	11	807	1.23	1.21
W163-B	1.19	5.05	0.20	9	921	1.48	1.13

for Run W112. A step increase of shock pressure to a constant level was common and the rise times were fractions of a millisecond. The duration of the uniform shock pressure of over 4 ms is also shown. The corresponding photographic response of Wood's metal is shown 2-dimensionally in Fig. 3. The time separation between each frame is 410 μs. There was no obvious difference in drop response between Wood's metal and mercury. Drop flattening occurs until the sixth frame when significant volume increase is noticed. At the 12th frame, the leeward side of the drops had a rough appearence, but th windward surface remained smooth. The spike shape, which resembles the Taylor

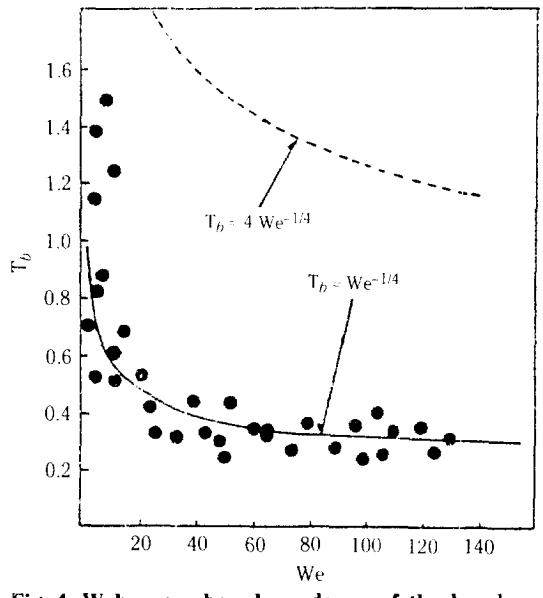

Fig. 4. Weber number dependency of the breakup time.

instability, becomes more apparent in the subsequent frames. Unstable surface waves by Taylor instability theory are predicted by Harper et al. [5] on the windward surface of the drop. Unlike hydrodynamic fragmentation in liquid-gas systems, where the boundary-layer stripping mode of breakup is common, neither misty wakes nor peeling off small droplets from the drop edge were observed. Instead, the drop volume increased continuously, suggesting continuous coolant entrainment into the drop conglomerate. Table 2 lists the present experimental results. The dimensionless breakup time, T_b, is based on equal volume mixing of the drop and coolant. The Weber number dependency of the breakup time is shown in Fig. 4. The correlation between the Weber number and the breakup time has some scattering. However, the one time constant

$$T_b = We^{-1/4} \tag{3}$$

is a good representation for the experimental data though some data show uncertainties. Because all drops (except M159-A) analyzed have shown fragmentation behavior, the threshold values of Weber numbers are not conclusively decided. Nonetheless, a critical Weber number, $We_{cr} = 10$ is tentatively assumed.

The displacement data for each drop were obtained from high-speed movies and a least square fit was applied to a correlation of the following form

$$x = pt^q + u_{do}t \tag{4}$$

where p and q are nonlinear regression parameters

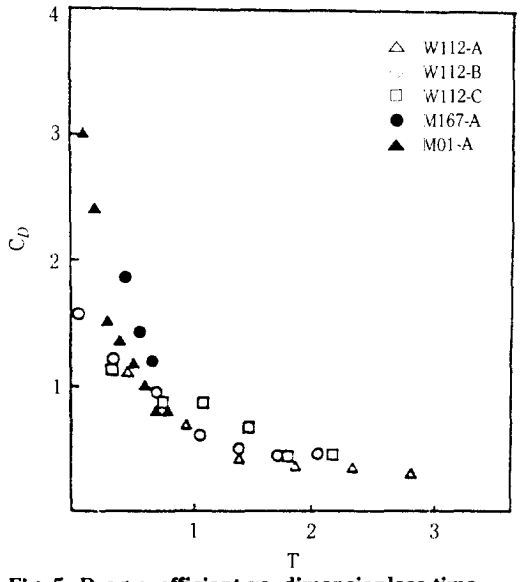

Fig. 5. Drag coefficient vs. dimensionless time.

and u_{do} is the initial drop velocity before the shock arrives. The terminal velocity of a drop can be determined by high-speed movies and is about 60 cm/sec. Since we know at any instant the values of x, dx/dt, and d^2x/dt^2, the equation of motion for a deforming fuel drop can be written as

$$\frac{d}{dt}\left[\left(\rho_d+\frac{1}{2}\rho_c\right)V_d\dot{x}\right]=C_D\left[\frac{\rho_c u_r^2(t)}{2}\right]A_d \qquad (5)$$

where both the drop density, ρ_d and the volume, V_d are functions of time. A_d is the projected area of a drop, assuming an axisymmetric body, and $u_r(t)$ is the relative velocity, $u_2(t)-u_d(t)$, where both liquid velocity and drop velocity vary with time. Virtual mass effects also have been included.

In Fig. 5, the drag coefficients estimated by Eq. (5) for several experiments are plotted against dimensionless time. The asymptotic behavior for large times is:

$$C_D=C_{Di}\exp(A\cdot T) \qquad (6)$$

where C_{Di} and A are found by best fit of data. The nonlinear regression gives $C_{Di}=3.54$ and $A=-1.33$ for mercury, and $C_{Di}=1.0$ and $A=-0.61$ for Wood's metal. The drag coefficients based on initial values of drop mass and acceleration are consistently higher in the mercury experiments than in Wood's metal experiments. The values for Wood's metal were in the range from about 1 to 2.5, and for mercury from 3.0 to 10. The scatter of the data is probably due to the sensitivity of the C_D values to the initial acceleration. The

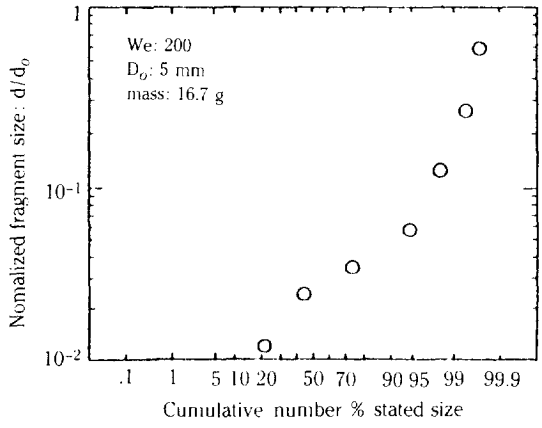

Fig. 6. Fragment size distribution (cumulative form).

acceleration was calculated from displacement data of the initially free-falling drops subject to a shock-induced flow. In analysis of the high speed movies, the time origin at which the incident shock hits the drop windward surface introduces uncertainty.

Fig. 6 shows the cumulative fragment size distribution for Wood's metal experiments. The Weber numbers were estimated to be about 200, based on 5 mm initial drop diameters. Experiments with the same conditions were repeated ten times in order to increase the mass collected. The total mass accumulated was 17.65 g. Screen meshes of six different sizes were used to measure the particle size distribution. The number median fragment size was compared with existing data for drop breakup in gas flows. The present experimental data were comparable with the data of Wolfe [11], who conducted a comprehensive study on fragment size distributions for a wide range of Weber numbers. Wolfe used photomicrographs of the slides in measuring fragment sizes which resulted from the breakup of 1.6-2.7 mm diameter liquid drops in gas flows. The minimum particle size reported by Wolfe was 6 μm, while the present data indicate the smallest fragment size of about 50 μm. Wolfe's mass mean fragment size for We = 200 was about 60 μm based on a 1.6 mm initial drop diameter. The mass median fragment size of the present data is around 300 μm. However, considering non-spherical fragment shape in the present experiment, the effective particle size would be smaller. The particle sizes can be theoretically considered as follows.

Since the cut-off wave length, λ_{cut}, for the Taylor instability is

$$\lambda_{cut}=2\left[\frac{\sigma}{a(\rho_f-\rho_c)}\right]^{1/2} \qquad (7)$$

In terms of the Weber number,

$$\lambda_{cut}=2\left[\frac{2}{3}\frac{d_o^2}{C_D(1-\varepsilon)We}\right]^{1/2} \tag{8}$$

Hence, for a 5 mm droplet with $C_D=2.0$ and We = 200, the primary cutoff wavelength is calculated to be 1.37 mm, and the fastest-growing wavelength is over 2.0 mm. These facts do not either support the Taylor instability as the principal mechanism governing liquid drop fragmentation in the present experiment. The dimensionless breakup time was about 1.5, which corresponds to the fragmentation time of 2 msec. Thus breakup was completed before the reflected wave hit the drop, based on the doubling of the apparent volume. It should be pointed out that the introduction of steel wool was effective in minimizing the influence of the reflected shock.

ENTRAINMENT MODEL

Observations of the high-speed photographs reveal that the apparent volume expansion occurs continuously during and following the drop flattening. The drop flattening is caused by the pressure differences between the equator region and the stagnation point area. Drop volume is increased by the entrainment of water into the metal. Since the main concern in Fuel-Coolant Interactions (FCI) is the rate of energy transfer through mixing and fragmentation, a simplified model is proposed to predict the gross behavior of the fuel droplet.

1. Model

The average motion of liquid drops in the shock-induced flow is considered with the following assumptions.

1. The drop initially has a downward velocity which is the terminal velocity of a drop through two-phase mixture.

2. The continuous phase has a uniform velocity, u_2, in the same direction as the droplet.

3. The drop is assumed as an axisymmetric body and has an equivalent radius, R.

4. The rate of mass entrainment into a drop is proportional to the relative velocity between the dispersed and continuous phases.

5. The rate of mass entrainment is also proportional to the surface area of a droplet, which is estimated by the equivalent spherical radius.

In view of the above assumptions, the equation of motion for the drop can be written as

$$\frac{d}{dt}\left(\frac{4}{3}\pi R^3\rho_d u_r\right)=-g(\rho_d-\rho_c)\frac{4}{3}\pi R^3 - \frac{1}{2}C_D\rho_c u_r^2\pi R^2 \tag{9}$$

where

$$\rho_d=\rho_c+(\rho_f-\rho_c)\frac{R_o^3}{R} \tag{10}$$

and g is the acceleration due to gravity, C_D is the effective drag coefficient and u_r is the relative velocity between the shock induced liquid velocity (u_2) and the drop velocity (u_d). R is the equivalent spherical radius of a drop which is a function of time.

According to the assumptions (4) and (5), an entrainment coefficient, E_{cf} is defined by

$$\frac{dM}{dt^+}=4E_{cf}\rho_c\pi R^2 u_r \tag{11}$$

where M is total mass of the drop, and E_{cf} is a function of the relative velocity and the changing drop radius. $t^+(=t-t_q)$ is the time when drop starts to show apparent expansion, t is the real time after shock hits the drop, and t_q is the delay time. The delay time, t_q depends on the initial surface perturbation as well as the effects of oxidation and solidification. Thus, it is apparent that

$$\frac{dM}{dt^+}=0 \quad \text{for } t^+<0. \tag{12}$$

Since the rate of change of total drop mass is the same as the rate of mass entrainment of liquid coolant into the drop,

$$\frac{dM}{dt}=4\pi\rho_c R^2\cdot\frac{dR}{dt}. \tag{13}$$

Thus, Eqs.(9) to (13) comprise a system of differential equations which can be solved with the initial conditions: $u_r(0)=u_{ro}$; $R(0)=R_0$; $\rho_d(0)=\rho_f$. An IMSL routine in the VAX 750 was utilized to solve the system of differential equations (9) through (13).

2. Comparison with Experimental Data

For experiments below the critical Weber number, drops oscillate all the time without expansion. When the Weber number exceeds a critical value, drop responses to the shock wave can be classified into two types. The former type showed continuous volume increase right after shock impact on the drop. In the latter type of interaction, the experimental data for drop volume history did not show significant change during the initial stage. After quiescent period of insignificant volume change, the apparent volumes showed sudden substantial and continuous increases from their original values. These phenomena confirm the observations made by Patel and Theofanous [8]. These authors referred the definition of breakup time to this behavior so that the breakup time was based on the initiation of breakup rather than on complete disintegration. Engel [12], in her work on waterdrop breakup behind an air shock, also noted the existence

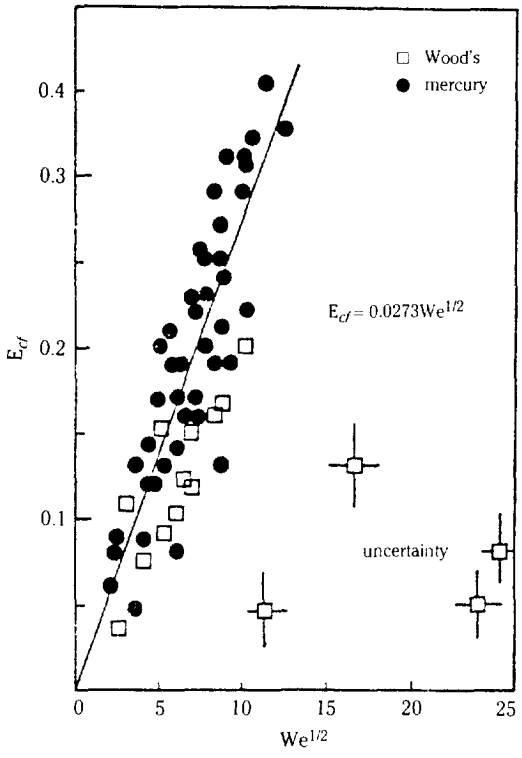

Fig. 7. Weber number vs. entrainment coefficient.

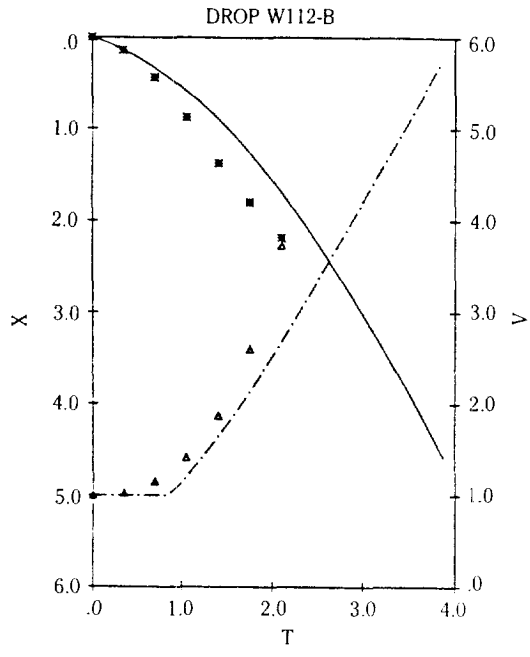

Fig. 8. Dimensionless displacement and apparent volume ratio as a function of dimensionless time for W112-B, We = 83: *, displacement, △, volume.

of the period of apparent quiescence. In the present experiment, this period corresponds with the time during which only drop flattening occurs. The above two different types of interaction might be attributed to the mode of molten metal drop formation technique. In experiments with small spherical drops, surface tension forces dominate over inertia before substantial flow fields are developed so that no entrainment occurs. For larger drops with initial deformation, turbulent mixing between the drop and coolant begins immediately after the shock arrival.

In order to calculate the average value of entrainment coefficients from experimental data, the following method was used:

$$E_{cf} = \frac{1}{t_e}\int_0^{t_e} E_{cf}(t)\,dt \tag{14}$$

t_e is the velocity equilibrium time when the drop velocity reaches 60% of the initial value of shock-induced liquid velocity.

In Fig. 7, the average entrainment coefficients are plotted against square root of Weber numbers. While some scatter is shown in the figure, the graph still shows that the entrainment coefficient is an increasing function of Weber numbers. There are at least four data points of uncertainty (W303-A, W303-B, W324-A, W112-C). The uncertainties might have come from either the solidification effect or oxidation in the Wood's metal experiments. A least square fit to a linear function gives a correlation of the form with a correlation coefficient of 0.73.

$$E_{cf} = 0.0273We^{1/2} \tag{15}$$

where $E_{cf} = 0$ was assumed for $We = 0$ and the four uncertain data were excluded in the calculation. In a turbulent model for the motion of buoyant thermal, Wang [13] suggested the entrainment coefficients of the form

$$E_{cf} = 0.025 + 0.31C_D' \tag{16}$$

where C_D' is the effective form drag coefficient. Previously reported experimental values on the entrainment coefficient are $E_{cf} = 0.25$ [14] and $E_{cf} = 0.014$ [15]. Considering different physical conditions from which E_{cf} was deduced, Eq. (15) was used to compare the drop interaction data in the present experiment with the model prediction.

Fig. 8 and 9 show the results of the dimensionless displacement and the apparent volume ratio for Drop W112-B and M174-A. Using the effective drag

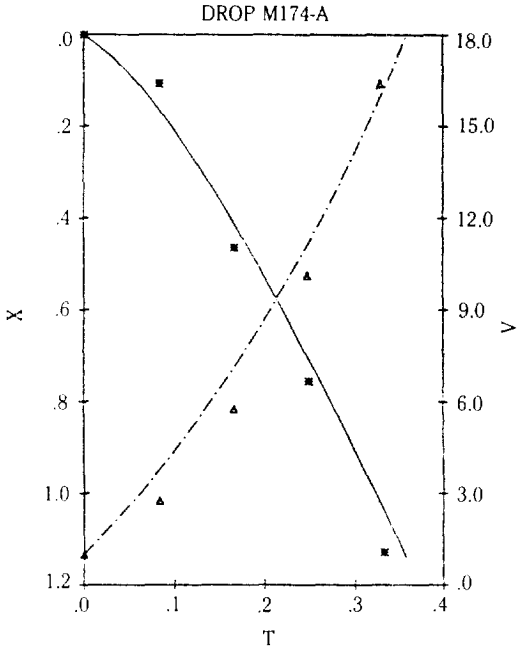

Fig. 9. Dimensionless displacement and apparent volume ratio as a function of dimensionless time for M174-A, We = 27: *, displacement, △, volume.

coefficient $C_D = 1.0$ for Wood's metal and $C_D = 2.5$ for mercury, and Eq. (15) for the entrainment coefficient, the model solutions and experimental results are in good agreement for both the displacement rate and the volume change. It should be remarked that, in predicting experimental data for drop volume history with the apparent initial quiescent period, the model must have utilized a parameter, t_q. This delay time, t_q is explicity included in the computer program so that the volume expansion begins at $t = t_q$. t_q is due to the initial drop deformation along with the solidification and oxidation of Wood's metal. No efforts have been made to find a correlation for this delay from the present experimental data. For drops which do not have the quiescent period, the calculation for volume change begins upon shock arrival.

CONCLUSIONS

Fragmentation of liquid drops behind a pressure shock wave has been experimentally investigated in a shock tube geometry. Photographic sequence of drop responses for Wood's metal and mercury revealed that drop expansion occurred due to the coolant mass entrainment into the drop. The one time constant represents well the correlation between $We^{-1/4}$ and T_b, the breakup time which was defined as the time when the apparent volume increased twice the initial drop volume. Fragment size measurements showed that the time constants for the Taylor instability were too big to generate the particle size distribution obtained in the experiment.

An entrainment model was developed to predict the rate of drop volume increase and the drop displacement. By uitilizing two parameters, E_{cf}, the entrainment coefficient, and C_D, the effective drag coefficient, the present model seemed to predict quite well the drop fragmentation processes. The drop volume history and the drop trajectory were reasonably well fitted by the effective drag coefficient $C_D = 2.5$ and the correlation of the form $E_{cf} = 0.0273\ We^{1/2}$. This suggests that the hydrodynamic fragmentation can be studied well by the concept of mass entrainment so that the rate of energy transfer through mixing and fragmentation can be predicted. However, this entrainment correlation should be used with caution since the initial drop perturbations might have played a role on the rate of coolant entrainment into the drop. Future works can include the viscosity effect on the entrainment so that the Reynolds number is formally contained in the correlation.

ACKNOWLEDGEMENT

This work was partially supported by the Korea Science and Engineering Foundation.

NOMENCLATURE

A : projected area [m^2]
a : acceleration [m/s^2]
Bo : Bond number, $\rho_c a d_o^2 / 4\sigma$ [-]
C_D : drag coefficient [-]
d : drop diameter [m]
E_{cf} : entrainment coefficient [-]
g : gravitational acceleration [m/s^2]
M : mass of drop [Kg]
p,q : regression parameter [-]
R,r : radius [m]
T : dimensionless time, $(tu_r/d_o)\varepsilon^{1/2}$ [-]
t : time [s]
u_2 : liquid velocity [m/s]
u : velocity [m/s]
u_{do} : initial drop velocity [m/s]
V : dimensionless volume, v/v_o [-]
v : volume
We : Weber number, $\rho_c u_r^2 d_o / 2\sigma$ [-]
X : dimensionless displacement, X/d_o [-]
x : displacement [m]

Greek Letters

ε : density ratio, ρ_c/ρ_f [–]
λ : wave length [m]
ρ : density [Kg/m^3]
σ : surface tension [N/m]

Subscripts

b : breakup
c : coolant; continuous phase
d : drop; dispersed phase
f : fuel
r : relative
o : initial

REFERENCES

1. Bankoff, S.G.: Proc. 6th Int. Heat Transfer Conf., Toronto, Canada, **6,** 355 (1978).
2. Fauske, H.K.: *Nucl. Sci. Eng.*, **51,** 95 (1973).
3. Board, S.J., Hall, R.W. and Hall, R.S.: *Nature*, **254,** 319 (1975).
4. Ranger, A.A. and Nicholls, J.A.: *AIAA J.*, **7,** 285 (1969).
5. Harper, E.Y., Grube, G.W. and Chang, I.-Dee: *J. Fluid Mech.*, **52,** 565 (1972).
6. Simpkins, P.G. and Bales, E.L.: *J. Fluid Mech.*, **55,** 629 (1972).
7. Reinecke, W.R. and Waldman, G.: 3rd Int. Conf. on Rain Erosion and Related Phenomena, Hampshire, England (1970).
8. Patel, P.D. and Theofanous, T.G.: *J. Fluid Mech.*, **103,** 307 (1981).
9. Baines, M. and Buttery, N.E.: CEGB Report RD/B/N/4643 (1979).
10. Kim, D.S., Burger, M., Frohlich, G. and Unger, H.: Int. Mtg. on LWR Severe Accident Evaluation, ANS/ENS, Boston, MA (1983).
11. Wolfe, H.E. and Anderson, W.H.: AGCD Report No. 0395-04 (1964).
12. Engel, O.G.: *J. Research of the National Bureau of Standards*, **60,** No. 3 (1958).
13. Wang, C.P.: *Phys. Fluids*, **16,** 744 (1973).
14. Scorer, R.S.: *J. Fluid Mech.*, **2,** 583 (1957).
15. Taylor, G.I.: *Proceeding Royal Society, London*, **201,** 159 (1950).